Localization of Point Source Scatterers from Ultrasound Images

Kaitlyn Liang

Abstract—This report delves into the precise localization of point source scatterers from ultrasound images, showcasing a novel approach that surpasses traditional methods by targeting sub-0.5 mm precision. By leveraging the Field II ultrasound program, which employs the Tupholme-Stepanishen method, this study simulates complex ultrasound fields and interactions with scatterers. The study embarks on minimizing the differences between simulated and ground truth images to pinpoint scatterer locations with unprecedented accuracy. The investigation reveals the critical role of dynamic range management and the intricacies of beam focusing in enhancing image resolution and scatterer localization. By methodically altering scatterer positions and employing focused transmit beams, the research identifies the focal length's significant impact on localization precision. The findings indicate an improvement in both lateral and axial resolutions for scatterers positioned outside the focal zone, demonstrating the potential of this methodology to extend ultrasound imaging capabilities into the realm of super-resolution. Despite its promising results, the study acknowledges limitations, particularly the reliance on initial guess accuracy and the challenges posed by complex ultrasound data landscapes. Furthermore, it underscores the necessity for advanced optimization techniques to tackle the inherent difficulties in localizing multiple scatterers, a common scenario in real-world ultrasound imaging. In summary, this research not only advances our understanding of ultrasound imaging mechanics but also paves the way for future developments in super-resolution imaging techniques, promising significant implications for medical diagnostics and treatment planning.

1 Introduction

Ultrasound (US) imaging, also known as sonography, is a non-invasive diagnostic medical imaging technique that uses high-frequency sound waves to produce images of structures within the body. An ultrasound transducer, composed of many piezoelectric (PZT) crystals will individually transmit ultrasound waves when an AC voltage is applied. When activated, a PZT crystal will create a spherical wave that propagates through the medium. These PZT crystals can be electronically controlled to focus, and steer the ultrasound wavefront. These US waves will travel through the medium until it is reflected back by a tissue boundary or a point scatterer. The reflected wave is detected by the PZT crystals that convert the mechanical vibrations into electrical signals in the form of radio frequency time series data. The time it takes for the echoes to return and their relative strength are used to create real-time images.

US imaging is widely used in medicine for examining various parts of the body, such as the abdomen, heart, blood vessels, and the development of a fetus during pregnancy. It's particularly useful for its ability to provide live images, enabling dynamic examinations (e.g., heart movement and blood flow) and guiding procedures (e.g., needle biopsies). Ultrasound is favored for its safety, as it doesn't use ionizing radiation, its relative affordability, and its portability.

US images suffer from a finite spatial resolution determined by the diffraction limit of the sound wave. As a result, standard frequencies for US waves (5 MHz) will have a lateral resolution of approximately 0.5 mm. As a result, there is significant uncertainty when localizing objects less than 0.5 mm such as breast microcalcifications in the breast. Additionally, the US waves may undergo several phenomena such as differing speeds of sound, reverberation artifacts, or speckle noise that could cause inaccurate localization of ultrasound images. When focusing the US beam, scatterers that are not at the focal length often look distorted due to the lack of convergence in the transmitting beams. Localizing the accurate location of the scatterer is very important for needle guidance, treatment planning, and monitoring disease progression.

2 Related Work

Determining the ground truth and making quantitative measurements in ultrasound imaging is an emerging field with many clinical applications. Most research has been geared towards localizing macro-structures such as organs and tissue boundaries. An automated system was developed in 2015 to normalize ultrasound images, reduce speckle, and segment the carotid artery as a snake. The snake segmentation algorithm adapts by a dynamic process that minimizes an energy function that inputs the strength, tension, and stiffness parameters. This processing was implemented to perform intima-media thickness measurements, and provide differences between the left and right sides [1]. Energy-based methods have also been used to automatically segment lesion regions in liver ultrasound images [2].

Deep learning approaches have been utilized to perform automatic estimation of the spleen length from US images to determine the progression of splenomegaly among children with sickle cell disease (SCD). A segmentation model achieved a percentage length error of 7.42 percent which approaches the level of inter-observer variability

(5.47-6.34 percent) [3].

Another important approach is the Markov Random Field (MRF). This is a mathematical model that represents the spatial interactions and dependencies between variables or pixels in an image. The probabilistic model considers the likelihood of a pixel's state based on the states of its neighbouring pixels. An MRF-priors based model has been used to train ensemble segmentation processes that can avoid irregular shape, and isolated points and holes for breast tumor segmentation. [4]

These approaches have been applied to the B-mode image; the processed image that is the conventional way to display US data. These images involve such as delay-and-sum beamforming to develop the final image. However, the received radiofrequency data from the elements will have more details on the wave propagation because the signal can be tracked between different elements. The increase in time delay precision has enabled the tracking of individual microbubble contrast agents to perform ultrasound localization microscopy [5].

3 Description of Method

I want to expand this work by localizing point scatterers to sub-0.005 mm precision with a 5 MHz transducer. The plan is to use the radio frequency (RF) data received from the elements of a transducer to The Field II ultrasound program was used to simulate ultrasound transducer fields and imaging. The programs uses the Tupholme-Stepanishen method for calculating pulsed ultrasound fields. The program is capable of calculating the emitted and pulse-echo fields for both the pulsed and continuous wave case for a large number of different transducers. Additionally, scatterers can be placed in the path of the ultrasound wave, and the corresponding RF data will be generated.

The transducer parameters included 64 elements that are 290 um wide, and spaced 20 um apart. The total width of the transducer is therefore set to 2 cm. The impulse response of the transducer is set to 0.4 usec for maximum axial resolution. The beam is focused at 3 cm away from the transducer.

For maximum resolution, focused transmit beams are used to create the image. 85 beams are transmitted and received where the focal position in the x-direction shifts from -1 cm - 1 cm. In each transmit sequence, all 64 elements transmit to maximize the US intensity at a particular location, and all 64 elements receive signals for a subsequent period of time. Therefore, this focused transmit sequence involves 85 sets of the 64 elements' receive signals.

A ground truth scatterer was set at a certain position within the x range and z range of the transducer (0.5 cm from the centre, and 2.5 cm down). The RF data will be processed to form an image, and the following image will be used as the ground truth image. The goal of the project is to be able to guess the approximate location of the point scatterer. This is completed by randomly guessing a position of the scatterer (0-1 cm in the x-range, and 2-3 cm in the z-range). The location of the guess scatterer will be defined in Field II, and the corresponding RF data will be generated. The RF data is then processed to create an image. The L2 norm of the difference between the guess image, and the ground truth image is used as the loss function.

$$minimize_x ||b - Ax||_2^2$$

In this model, b is the ground truth image, x is the location of the guess scatterers, and A is the function that converts the location of the guess point scatterer to the image. Although A is technically a matrix, it is not differentiable, and it is expressed as a function in MATLAB where Field II is called to calculate the RF data. The complexities of the RF data generation and subsequent image generation makes A inherently non-differentiable. As a result, any optimization function that depends on the gradient of the function cannot be used in this case.

The fminsearch algorithm in MATLAB is used to minimize this unconstrained multivariable function. This function incorporates the Nelder-Mead simplex which operates on a geometric figure called a simplex, which is N dimensions in a shape with N+1 vertices. The algorithm iteratively refines the simplex to approximate the minimum of the function by reflecting, expanding, contracting, and shrinking the simplex. Although it is relatively simple to implement and apply to a wide range of problems, the algorithm is not optimized for higher dimensions and complex landscapes such as the localization of a hundred point scatterers. Other optimization methods such as nonlinear least squares was also implemented, but the fminsearch algorithm performed the best.

One of the big considerations with ultrasound data is the high dynamic range. The magnitude of the data will exhibit upwards of a 100 dB range. Any region of the picture with no or a very small gradient will cause the algorithm to get caught in local minima. As a result, the dB and gamma correction was applied to each image to reduce the dynamic range of values. The values of the image were then rescaled to be between 0 and 1. The B-mode, and the rescaled images of the ground truth point scatterer is shown in Fig. 1-10.

The rescaled images show curved lines coming from the scatterer. The three curved lines are a result of the multiple beams that are at different x-positions than the actual scatterer. These lines are necessary for the fminsearch algorithm to move the scatterer closer to the ground truth point source location.

The ground truth scatterer was moved relative to the focal length of the transducer. The localization of the point scatterer varied heavily on the initial guess of the scatterer, so the algorithm was run 200 times for each ground truth location. 5 ground truth locations were used where the axial position moved at increments of 0.05 m. The axial position was moved to determine the effect of focus on the localization on the point scatterer. In each run, a location of a scatterer is randomly chosen, and the algorithm adjusts

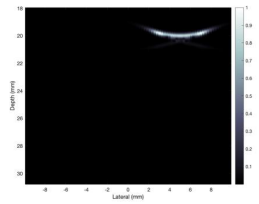

Fig. 1. B-mode image of Point Scatterer at Depth of 0.02 m

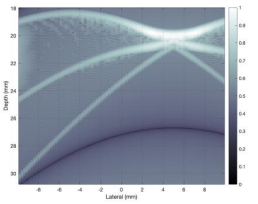

Fig. 2. Rescaled B-mode image of Point Scatterer at Depth of 0.02 m

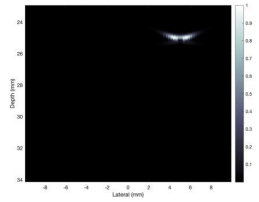

Fig. 3. B-mode image of Point Scatterer at Depth of 0.025 m

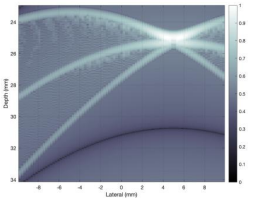

Fig. 4. Rescaled B-mode image of Point Scatterer at Depth of 0.025 m

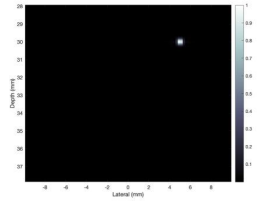

Fig. 5. B-mode image of Point Scatterer at Focal Length (0.03 m)

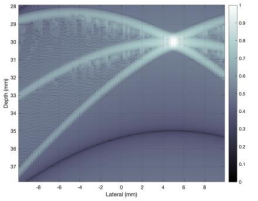

Fig. 6. Rescaled B-mode image of Point Scatterer at Focal Length (0.03 m)

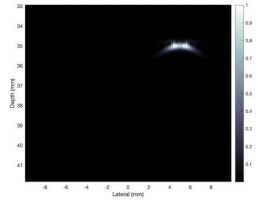

Fig. 7. B-mode image of Point Scatterer at Depth of 0.035 m

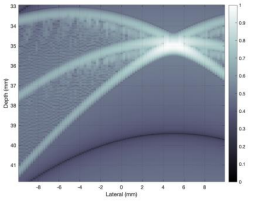

Fig. 8. Rescaled B-mode image of Point Scatterer at Depth of 0.035 m

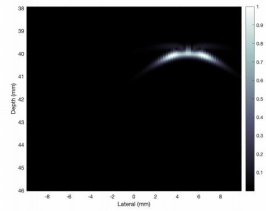

Fig. 9. B-mode image of Point Scatterer at Depth of 0.04 m

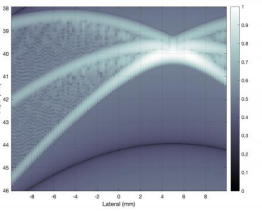

Fig. 10. Rescaled B-mode image of Point Scatterer at Depth of 0.04 m

the x and z position of the scatterer until it converges. The location of the guess was limited to +/- 0.005 m away from the ground truth in the lateral direction and axial directions. These values were normalized to 0 and 1. The final location with the smallest L2 norm was determined to be the closest. The location of the ground truth scatterer is at the center of each figure.

4 Analysis and Evaluation

In each iteration, the initial and final location of the guess scatterer, and the L2 norm was recorded. The initial and final displacements were plot, and the hue of the scatterers is an indicator of the L2 norm value. The results are shown in Figures 11-20. The initial lateral and axial ranges of the random scatterers are used to determine the range of x and z-positions that allow the algorithm to achieve the right localization. The initial lateral and axial resolutions refer to the standard deviation of the PSF of the GT images. The final lateral and axial ranges are a measure of the algorithm's resolution. Any coordinate that has corresponds to an L2 norm of 10 or below is assumed to have the correct localization. The standard deviation of these x and z coordinates are taken to determine the initial and final resolution in the lateral and axial directions. The results are shown in Table 1.

Fig. 11-20, and Table 1 indicate the algorithm will localize any random scatterer within approximately a 3 mm radius from the ground truth. Any guess that is outside of this radius will converge at a local minimum. However, Table 1 indicates the algorithm will only localize a scatterer 1.7 mm away from the ground truth when the ground truth is at the focal length (3cm). This limitation may be attributed to the general symmetry of the point in focus. Any out-of-focus point will exhibit an intensity distribution with a larger standard deviation due to the lack of focus. Since the point in the focus has a smaller standard deviation, random scatterers must be closer to the ground truth location in order for the algorithm to converge at the global minimum.

Within the 3 mm range, the axial and lateral position of the guess scatterers were adjusted to be closer to the ground truth location. As a result, the change in resolution from the B-mode image to the localization algorithm increased by an order of magnitude for any point out-of-focus. The largest final lateral and axial resolution (1.2 mm, 0.19 mm) occurred when the ground truth location was at the focal length (3 cm). In the axial direction, the ground truth scatterer has the largest axial range due to the reflected beams coherently adding from similar beam angle. While the out-of-focus GT scatterers have some assymetry in the horizontal axis, the in-focus GT scatterer is only assymetrical at regions where the intensity is low. As a result, similar L2 norm will result from a location along the higher intensity lines close to the GT scatterer.

From the results in Table 1, the axial and lateral resolution increases when the scatterer is farther from the focal length of the beam. The axial resolution exhibits a

TABLE 1
An Example of a Table

GT Axial Position [cm]	2	2.5	3	3.5	4
Initial Lateral Range [mm]	2.7	3	1.7	2.6	2.9
Initial Axial Range [mm]	2.6	2.1	3.1	2.6	2.7
Initial Lateral Resolution [mm]	5	2	0.5	2	5
Initial Axial Resolution [mm]	2	2	2	2	2
Final Lateral Resolution [mm]	0.57	0.8	1.2	0.78	0.71
Final Axial Resolution [mm]	0.06	0.09	0.19	0.09	0.06

major increase due to the larger set of angles the US beams are hitting the scatterer. The lateral resolution is a result of the strong curvature in the peak intensity. When the scatterer is placed farther from the focal length (3-5 cm away), the intensity of the scatterer will lower, and result in significantly more lateral blurring. As a result, the lateral resolution will be significantly lower. The axial resolution will stay in the same range.

When observing the locations of the final displacements, the axial resolution is approximately 1 order of magnitude lower than the lateral resolution. This result can be attributed to the geometry of the scatterer in the B-mode images. In these images, the scatterer tends to exhibit lateral blurring due to the US beam transmission. This is caused by the beam focusing at a position lateral to the point scatterer, so the wavefront is hitting the point scatterer diagonally. The lateral blurring creates a wider signal that cause the L2 norm to converge at a wider lateral range. As a result, the L2 norm value is less sensitive to lateral changes as opposed to changes in the axial direction.

5 Conclusion and Discussion

From Fig. 11-20 and Table 1, the algorithm was able to localize a random scatterer to the GT location within an approximately 3 mm range. The largest lateral resolution achieved was 0.71 mm in the lateral direction, and 0.06 mm in the axial direction. At the focal length, a point scatterer exhibits a lateral resolution of 0.5 mm, and an axial resolution of 0.2 mm. However, the focus of the scatterer severely degrades at distances farther away from the focal length. Although the algorithm did not perform better than the B-mode image itself at the focal length, it was able to greatly increase the lateral and axial resolution of out-of-focus point scatterers. When the GT point scatterer was at 0.2 cm, the algorithm was able to decrease the lateral resolution from 5 mm to 0.57 mm. The axial resolution decreased from 0.2 mm to 0.06 mm. These results indicate that out-of-focus point scatterers can be localized to a position that exceeds the diffraction limit of the system. Exceeding the diffraction limit can expand the ultrasound imaging field to super-resolution ultrasound imaging without the use of contrast agents.

Dynamic receive focusing accomplishes a similar goal by only taking the time points of certain elements in a transducer corresponding to the location. However, this method decreases the signal intensity of the point scatterer

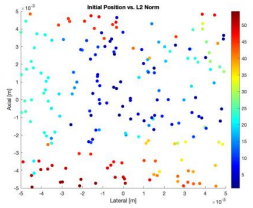

Fig. 11. Initial Displacement of Guess Scatterers where GT Depth=0.02 m.

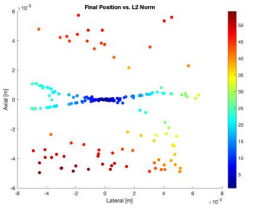

Fig. 12. Final Displacement of Guess Scatterers where GT Depth=0.02 m.

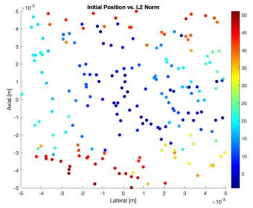

Fig. 13. Initial Displacement of Guess Scatterers where GT Depth=0.025 m.

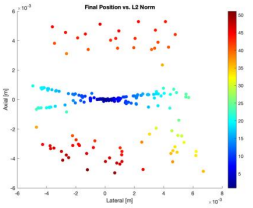

Fig. 14. Final Displacement of Guess Scatterers where GT Depth=0.025 m.

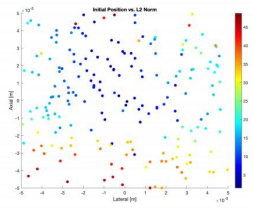

Fig. 15. Initial Displacement of Guess Scatterers where GT Depth=0.03 m.

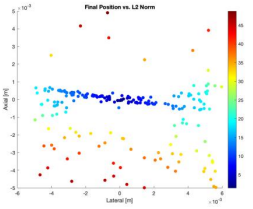

Fig. 16. Final Displacement of Guess Scatterers where GT Depth=0.03 m.

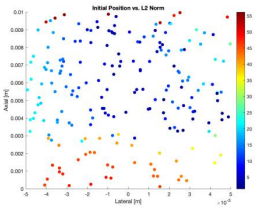

Fig. 17. Initial Displacement of Guess Scatterers where GT Depth=0.035 m.

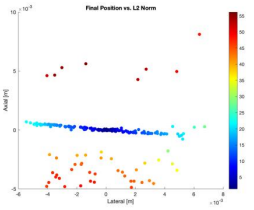

Fig. 18. Final Displacement of Guess Scatterers where GT Depth=0.035 m.

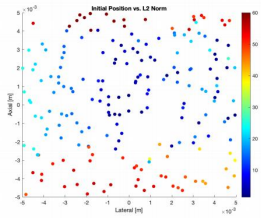

Fig. 19. Initial Displacement of Guess Scatterers where GT Depth=0.04 m.

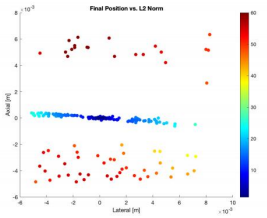

Fig. 20. Final Displacement of Guess Scatterers where GT Depth=0.04 m.

whereas all intensity values are used in our method.

One of the limitations of this method comes from the fminsearch algorithm itself. When localizing multiple scatterers, the algorithm takes significantly longer to converge, and it often converges to a local minimum. Although the goal of this project was to only localize one point scatterer, in vivo ultrasoud images tend to exhibit a large number of scatterers. Modifying or using a different optimization algorithm such as nonlinear least squares could be useful in these scenarios

Another limitation of this method is the accurate guessing required to converge at the global minimum. A 3 mm radius is very small in comparison to an image that has a field-of-view on the order of several cm wide. If applying this technique to real data, the location of the guess scatterer will have to come from the image itself.

Lastly, this technique was only applied to simulated data from Field II. The simulated data is a little unrealistic because the algorithm ignores the presence of diffuse scatterers, and non-uniform wave propagation in tissue. As a result, using Field II to determine the location of scatterers in a real image can incorrectly model the wave propagation in the tissue, and result in inaccurate localization.

ACKNOWLEDGMENTS

The author would like to thank Dr. Soon Wei Daniel Lim for being a great postdoc, and providing very helpful advice and moral support for this project.

REFERENCES

[1] K. M. Meiburger, U. R. Acharya, and F. Molinari, "Automated localization and segmentation techniques for b-mode ultrasound images: A review," *Computers in Biology and Medicine*, vol. 92, pp. 210–235, 2018. [Online]. Available: https://www.sciencedirect.com/science/article/pii/S0010482517303888

[2] W. Wang, J. Li, Y. Jiang, Y. Xing, and X. Xu, "An automatic energy-based region growing method for ultrasound image segmentation," in *2015 IEEE International Conference on Image Processing (ICIP)*, 2015, pp. 1553–1557.

[3] Z. Yuan, E. Puyol Anton, H. Jogeesvaran, C. Reid, B. Inusa, and A. King, *Deep Learning for Automatic Spleen Length Measurement in Sickle Cell Disease Patients*, 10 2020, pp. 33–41.

[4] K. M. Meiburger, U. R. Acharya, and F. Molinari, "A cost-sensitive extension of adaboost with markov random field priors for automated segmentation of breast tumors in ultrasonic images," *Int J CARS*, vol. 5, pp. 537–547, 2010. [Online]. Available: https://link.springer.com/article/10.1007/s11548-010-0411-1#citeas

[5] G. S. Stefanie Dencks, "Ultrasound localization microscopy," *Z Med Phys*, vol. 3, pp. 292–308, 2023. [Online]. Available: https://www.ncbi.nlm.nih.gov/pmc/articles/PMC10517400/#:~:text=For%20localization%20using%20rf%2Dsignals,a%20larger%20aperture%20is%20advantageous.